

An online data analysis system of INTEGRAL telescope

A.Neronov,^{1,2} V.Savchenko¹, A.Tramacere¹, M.Meharga¹, C.Ferrigno¹, and S.Paltani¹

¹ Department of Astronomy, University of Geneva, Ch. d'Ecogia 16, 1290, Versoix, Switzerland

² APC, University of Paris, CNRS/IN2P3, CEA/IRFU, 10 rue Alice Domon et Leonie Duquet, Paris, France

ABSTRACT

Context. During more than 17 years of operation in space INTEGRAL telescope has accumulated large data set that contains records of hard X-ray and soft γ -ray astronomical sources. These data can be re-used in the context of multi-wavelength or multi-messenger studies of astronomical sources and have to be preserved on long time scales.

Aims. We present a scientific validation of an interactive online INTEGRAL data analysis system for multi-wavelength studies of hard X-ray and soft γ -ray sources.

Methods. The online data analysis system generates publication-quality high-level data products: sky images, spectra and light-curves in response to user queries that define analysis parameters, such as source position, time and energy interval and binning. The data products can be requested via a web browser interface or via Application Programming Interface (API) available as a Python package. The products for the ISGRI instrument of INTEGRAL are generated using the Offline Science Analysis (OSA) software which is provided by the instrument teams and is conventionally used to analyse INTEGRAL data. The analysis workflow organized to preserve and re-use various intermediate analysis products, ensuring that frequently requested results are available without delay. The platform is implemented in a Docker cluster which allows operation of the software in a controlled virtual environment, and can be deployed in any compatible infrastructure.

Results. We report the functionalities and performance of the online data analysis system by reproducing the benchmark INTEGRAL results on different types of sources, including bright steady and transient Galactic sources, and bright and weak variable extra-galactic sources. We compare the results obtained with the online data analysis system with previously published results on these sources. We also discuss limitations of the online analysis system.

Conclusions. We consider the INTEGRAL online data analysis as a demonstrator of more general web-based “data analysis as a service” approach that provides a promising solution for preservation and maintenance of data analysis tools of astronomical telescopes on (multi)decade long time scales and facilitates combination of data in multi-wavelength and multi-messenger studies of astronomical sources.

1. Introduction

The International Gamma-Ray Laboratory (INTEGRAL) (Winkler et al. 2003) is an ESA space astronomy mission that has collected data in orbit since 2002. It provides observations of astronomical sources in the keV-MeV energy range. IBIS, the Imager on Board the INTEGRAL Satellite (Ubertini et al. 2003), is a coded-aperture instrument that provides fine imaging (12' FWHM) in a nearly squared partially coded field-of-view (FoV) of $30^\circ \times 30^\circ$, source identification and spectral sensitivity to both continuum and broad lines between 15 keV and 10 MeV. Its focal plane is composed of two detectors, optimized for two different energy ranges: ISGRI from 15 to ~ 1000 keV (Lebrun et al. 2003) and PICsIT from 400 keV to 10 MeV (Labanti et al. 2003). In the following, we will discuss only the ISGRI detector layer, and refer to it as the ISGRI instrument. The Joint European X-Ray Monitor (JEM-X Lund et al. 2003) provides images, timing, and spectral information in a lower energy range (3–25 keV). It has a narrower circular FoV $\sim 10^\circ$ diameter. The spectrometer SPI (Vedrenne, G. et al. 2003) provides high-resolution spectroscopy data with moderate angular resolution. The SPI instrument is surrounded by an Anti-Coincidence Shield (ACS) that reduces the level of background in SPI and simultaneously works as an all-sky Gamma-Ray Burst (GRB) monitor (Savchenko et al. 2012). The wide FoV of IBIS inherently includes data on a large number of astronomical sources, which are not necessarily the targets of specific observational proposals. This means that all source-specific observational campaigns of INTEGRAL pos-

sess large potential for serendipitous science. All INTEGRAL data become publicly available after a one-year proprietary period, so that analysis of all the sources found in the field of view is possible.

Astronomical sources visible in X-ray and soft γ -ray band are variable on different time scales, from milliseconds to years and decades. In this respect, the 17-year-long data-set of INTEGRAL is unique, as it contains the information on long-term variability patterns of a large number of sources. Some sources spend long periods in quiescent states producing little emission and exhibit occasional outbursts or flares on irregular basis with a duty cycles spread over years or decades. The INTEGRAL archive contains information on previous history of quiescence and activity of all sources, including those which might undergo outbursts in future.

The INTEGRAL data and Offline Science Analysis (OSA) software that includes data analysis pipelines for all instruments, including ISGRI (Goldwurm, A. et al. 2003) and JEM-X (Westergaard, N. J. et al. 2003) is distributed by the INTEGRAL Science Data Centre (ISDC) (Courvoisier et al. 2003). The main components of OSA have been developed in the period preceding the INTEGRAL launch and are maintained by ISDC. The architecture of OSA was optimized for computing environments that were common 20 years ago. INTEGRAL was initially planned to operate in space for five years and generate relatively small data sets. The only solution for data processing was via local installation of OSA on a user computer. This is not nec-

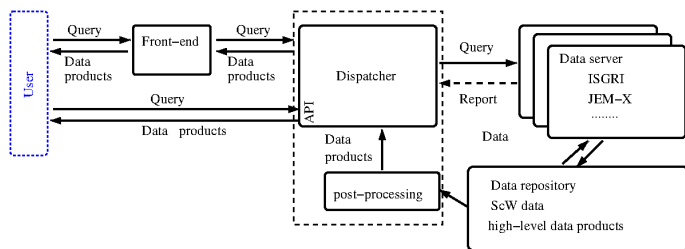


Fig. 1. Architecture of the INTEGRAL Online Data Analysis system.

essarily the case today for data sets spanning 17 years. Their analysis requires a significant amount of computing resources. Moreover, maintenance of legacy software on evolving operating systems poses more and more challenges.

The development of high-performance computing (HPC) and cloud computing (CC) technologies over the last decades opens up a new possibility of deployment of OSA-based data analyses without the need for local installation of the software, and provides access to large pool of computing resources, thus significantly reducing the complexity of the analysis of INTEGRAL data. Such online data analysis (ODA) system for the ISGRI instrument has been recently developed at the Common Data Centre Infrastructure (CDCI) of the University of Geneva¹ in synergy with the ISDC, and is maintained jointly with the François Arago Centre (FACe) of Astroparticle and Cosmology laboratory in Paris². In the following, we describe the system and characterize its performance via comparison of science results obtained using the system with previously published benchmark INTEGRAL results on a variety of Galactic and extra-galactic sources. We also demonstrate the usefulness of the system in the context of multi-wavelength studies and discuss advantages and limitations of this online data analysis implementation.

Throughout the paper, we provide direct links to the code producing the figures in the text, showing the potential of this approach for the open access, reusability and reproducibility of science results.

2. Online data analysis interface

The general scheme of the ODA is shown in Fig. 1. The user has several possibilities to submit requests for analysis of INTEGRAL data:

- through a web browser by accessing the CDCI website³ on his/her local computer and entering the analysis parameters into the parameter boxes, or
- directly specifying analysis parameters in a URL link to the CDCI website (examples are given in the next section) or
- through an ODA Application Programming Interface (API), `oda_api`⁴, e.g., from a Jupyter Notebook, also on his/her local computer.

The request arrives at a dispatcher, which interprets it and finds an appropriate data analysis service. The frontend and dispatcher API interfaces verify the correctness and completeness of user queries and process them through the dispatcher that forms requests to the data server(s) implemented as Docker⁵ containers

running OSA in service mode. The containers are currently deployed locally on the HPC resources of the University of Geneva, but they could be deployed on any other HPC or CC services.

Data products provided by the data server upon analysis requests are stored in a data repository and are made available to the dispatcher. In the current version of ODA, the dispatcher also performs post-processing and visualisation of the data products to be displayed on the front-end. This makes the results available to the user either through the front-end or through the API. The front-end displays sky images, spectra, light curves, and source catalogs in a virtual-desktop environment embedded in the web browser, providing the possibility to download the data products to the local user computer.

2.1. Front-end interface – Dispatcher – Data Server interactions

ISGRI and JEM-X are coded-mask instruments that rely on a dithering pointing strategy with individual exposures called Science Windows (ScW) lasting 0.1–1 hour. Reconstruction of sky images creates a catalog of detected sources. This should be used as an input for the extraction of spectra and light curves of specific sources, because this process requires a sky model in the form of a source list (see Goldwurm, A. et al. 2003, for details). The default ODA workflow allows the user to select the data set, obtain a catalog of detected sources by reconstructing an image, and then manipulate this catalog to extract spectra and light curves.

The data processing is initiated in response to the user queries defining the analysis parameters (Fig. 2). These queries include at the very minimum:

- Source name or sky coordinates
- Time interval for the data or Science Window (ScW) list

The front-end is able to resolve astronomical source names by accessing two of the main astronomical databases (SIMBAD and NED). It accepts time parameters in several different conventional formats. The list of ScWs can be specified as a comma-separated list of their unique identifiers. The ScW data base is separately accessible through the `w3browse` interface on the CDCI web pages⁶.

Apart from these generic query parameters, the front-end allows the user to specify parameters that are specific to the INTEGRAL instruments: ISGRI, JEM-X, SPI-ACS. An example of parameter field for ISGRI is shown in the right panel of Fig. 2. For ISGRI and JEM-X, it is possible to specify:

- one of the two currently used versions of OSA: 10.2 and 11.0;
- radius of the “region of interest” within which pointing data are selected (which depends on the instrument field-of-view);
- One of the two units of the JEM-X instrument (JEM-X1 or JEM-X2);
- type of the data product (image, spectrum or light curve);
- energy range of the image;
- minimal detection significance of sources in the output catalog from imaging;
- time binning for the light curve;
- source catalog to be used in spectral and timing analyses.

⁶ <https://www.astro.unige.ch/cdci/integral-archive>

¹ <https://www.astro.unige.ch/cdci/>

² <http://www.apc.univ-paris7.fr/FACe/home>

³ https://www.astro.unige.ch/cdci/astrooda_

⁴ https://github.com/cdcihub/oda_api

⁵ <https://hub.docker.com/r/odahub/ddosa-interface>

The figure shows two parts of the ODA front-end interface. On the left, the 'General parameter space' includes fields for 'Object name *' (Crab), 'RA *' (83.63308333), 'Dec *' (22.0145), 'Start time *' (2003-03-15T23:27:40.0), 'End time *' (2003-03-16T00:03:15.0), and 'Time unit' (ISO/IS). A 'Resolve' button is next to the object name field. Below these fields, it says 'Name resolved using Simbad (CDS, via client/server)'. 'Resolvers' are set to 'Local' and 'Sesame service'. On the right, an 'Instrument query parameters' panel for the ISGRI telescope shows 'OSA Version' (OSA10.2), 'Radius' (15), 'Use Science Windows - ScWs' (No), 'Energy Min *' (20), 'Energy Max *' (40), 'Query Type' (Real), 'Detection Threshold' (5), 'Product Type' (Image), and 'User catalog' (Choose file). A 'Submit' button is at the bottom.

Fig. 2. Left: General parameter space of ODA front-end. Right: example of instrument-specific parameter field for ISGRI telescope.

In a similar way, the parameters can also be specified in the API requests using the `oda_api` Python package. For example, OSA version is specifiable by setting a parameter `osa_version='OSA10.2'` in the API requests⁷.

The front-end provides a display of the high-level data products (images, spectra, light curves, source catalogues) through a virtual desktop environment. It also provides the possibility of performing post-analysis of the data, like, e.g., fitting spectra with XSPEC spectral models, using public domain rendering packages⁸.

2.2. Data analysis and storage organization

The ODA infrastructure is using the online archive of INTEGRAL raw data, provided by the ISDC⁹. The data server's task is to provide high-level data products corresponding to the user requests received through the dispatcher. Running OSA is time consuming (about 50 CPU-hours for a spectrum in a typical short transient observation, or of the order of 2000 CPU-hours for an analysis of historic data for a typical source), so as far as possible it is desirable to keep pre-computed products for future (re-)uses. However, it is not possible to store high-level data products for all imaginable combinations of user input parameters. In ODA, the permanent archive of the raw data is complemented by an analysis cache containing high- and intermediate-level data products that are added or removed depending on the the user demands averaged over certain time periods.

The cache storage is organized according to the data lineage (e.g. Ikeda & Widom 2009), which is a specific case of data provenance (Gupta 2009). The data lineage metadata comprises the information on the sequence of analysis steps (the analysis or workflow nodes) undertaken to produce given high- or intermediate-level data products. The ontology of the workflow

nodes prescribes specific metadata associated with each step, and induces the collection of metadata of the final product.

The lineage metadata of the cache storage contains all relevant properties of all stored data products, and only this information. This provides a possibility to re-use previously produced intermediate-stage data products for the processing of new data analysis requests by users. New data analysis workflows typically do not start processing of raw data from “from scratch”. Instead, they are formed from a combination of parts of already available workflows derived from specific intermediate or high-level data products stored in the cache, together with the provenance DAG metadata. This approach provides an efficient way to speed-up data processing following user requests if those are repetitive or recursive or if the requests are nearly identical to those done by previous users with only moderate parameter modifications.

Efficient reuse of parts of the OSA based data analysis workflow is enabled by the re-organisation of OSA in data analysis units expressed as Python classes, following the Declarative Data Analysis (DDA) approach inspired by the principles of functional programming. This development was driven by the needs of efficiently managing the data of INTEGRAL together with the information on the 17-year history of the telescope operations: by 2018, in the raw-data archive, there are about 10^3 different types of data occupying 20 TB in some 2×10^4 files.

The re-factored OSA implementing the DDA approach (called DDOSA¹⁰) follows a simple logical scheme suitable for reproducibility of the analysis. Each analysis unit is a pure function of its input data, meaning that it depends only on its own explicit input. It transforms the input data into other data products. Any data are uniquely identified by a tree of connected analysis units that were used to produce it, or, equivalently, by its DAG “provenance graph”. In other words, DDOSA uses provenance as a data identifier (see Savchenko 2020a, for more details).

The high-level data products associated to very large analysis chains may be eventually associated with a very large prove-

⁷ See `oda_api` documentation at <https://oda-api.readthedocs.io/en/latest/> for full details.

⁸ <https://bokeh.pydata.org/en/latest/>

⁹ <http://www.isdc.unige.ch/integral/archive>

¹⁰ See <https://github.com/volodymyr/ssa/dda-ddosa/> for implementation details.

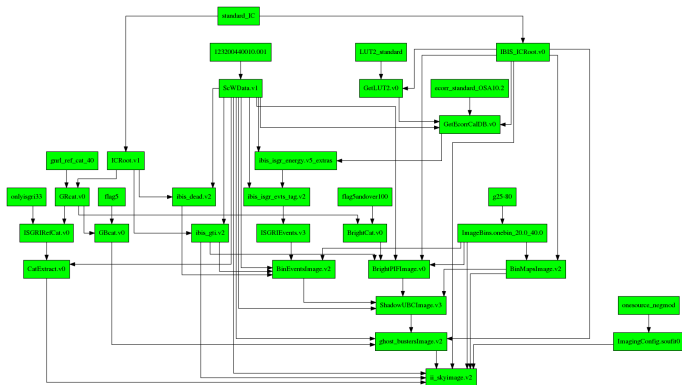


Fig. 3. Example of high-level provenance graph for a sky image derived from a single INTEGRAL ISGRI ScW.

nance graphs. An example of the provenance graph for a single ScW image high-level data product is shown in Fig. 3.

The DAG provenance graph approach for data identification at different analysis levels is optimal not only for caching frequently re-used intermediate analysis step results, but also for the parallelization of the analysis. The DAG structure of DDOSA workflows implies the presence of different independent branches of analysis that can be naturally executed independently in a distributed environment. This is taken into account in the system of job scheduling. For each analysis unit, execution requests originate either from the users (via dispatcher) or other analysis units. Each request processing starts from the evaluation of the request, resulting either in the retrieval of the requested products from the storage cache or in the delegation of the request to a local or remote executor, a process which is transparent from the point of view of the request. A simple scheduling layer has been implemented following this approach. The advantage of this scheduler is the straightforward treatment of complex dependencies.

3. Benchmark analysis results

The web-based ODA interface retains all the functionalities of OSA and could be used to obtain publication quality results of analysis of INTEGRAL observations with no difference from what an experienced user can obtain running locally OSA. In this section, we demonstrate the performance of the ODA based analysis on benchmark cases, by showing that the results obtainable with ODA are compatible with previously published results or improve on them, owing to upgraded algorithms and calibration.

3.1. Crab pulsar

The Crab pulsar and Nebula complex is one of the brightest sources on the X-ray sky (Hester 2008). Because of this property and its flux stability, it is often used as a “calibration” source in high-energy astronomy. INTEGRAL observations of Crab are reported in a number of publications (e.g. Mineo et al. 2006) and, in particular, in the context of the study of the long-term variability of the source emission (Wilson-Hodge et al. 2011). We verify the performance of ODA by reproducing the published results on Crab variability and extending the evolution study over a 15 year time period.

The ODA interface is currently limited to single requests for data analysis based on no more than 50 science windows

(ScWs), to limit the waiting time on the available resources (see Section 4 for details, future plans, and a work-around). If the requested time span of data extends over more than 50 ScWs, random selection of ScWs within the specified time limits is performed. This is the case for the results reported in Figs. 4, 5, and 6. The time interval of the analysis for this specific ScW subset is 2003-03-15 23:27:40.0 to 2018-03-16 00:03:15.0 UTC, spanning over more than 15 years. Pointings within 15 degrees from Crab position are selected.

Our example Crab image could be accessed or re-generated by directly re-launching the analysis via an URL <https://www.astro.unige.ch/cdci/astrooda/> in which the analysis parameters are specified after the sign {?} and separated by the {\&} sign as, for example: `src_name=Crab&RA=83.633080&DEC=22.014500&radius=15` for the source name and/or sky coordinates and region of interest specification, `&T1=2003-03-15T23:27:40.0&T2=2018-03-16T00:03:15.0&T_format=isot` for the time interval, `&E1_keV=20&E2_keV=40` for the energy interval, `&instrument=isgri&osa_version=OSA10.2&product_type=isgri_image` for the instrument, software version and data product specification (spaces are added for readability, but should be removed in the actual query). The parameter `detection_threshold=7.5` will result in display of the sources detected at significance level higher than 7.5. The analysis with specified parameters is launched automatically, as soon as the instrument parameter is defined: `&instrument=isgri`. The parameters that are not explicitly specified in the parameter field of the URL are fixed to their default values.

The URL executable URL with all specified parameters for each data product could be obtained by pressing the “Share” button displayed in the data product window on ODA frontend (see Fig. 4).

This example of analysis could also be launched from a python interface on the user laptop (e.g., from a shell or a Jupyter notebook) by providing parameters to the request

```
from oda_api.api import DispatcherAPI
disp=DispatcherAPI(
    host=
    'www.astro.unige.ch/cdci/astrooda/dispatch-data')
disp.get_product(
    RA=83.633080,
    DEC=22.014500,
    radius=15,
    T1='2003-03-15T23:27:40.0',
    T2='2018-03-16T00:03:15.0',
    E1_keV=20.0,
    E2_keV=40.0,
    instrument='isgri',
    product='isgri_image',
    osa_version='OSA10.2')
```

The API code for each data product can be obtained directly by pressing the “API code” button in the product window on the ODA front-end (see Fig. 4).

A crucial part of the imaging analysis is the search for significantly detected sources both in individual ScWs and in the mosaic image. Setting the source detection threshold to 7.5σ (a parameter in the web form of ODA) results, in our example, in the detection of four sources displayed in the image in Fig. 4. Details of the source detection are available in the catalog display accessible through a button from the image display panel, as shown in Fig. 4. Occasionally, sources may have multiple appearances in the catalog display, because this table combines several output catalogs of the standard INTEGRAL analysis, namely results of

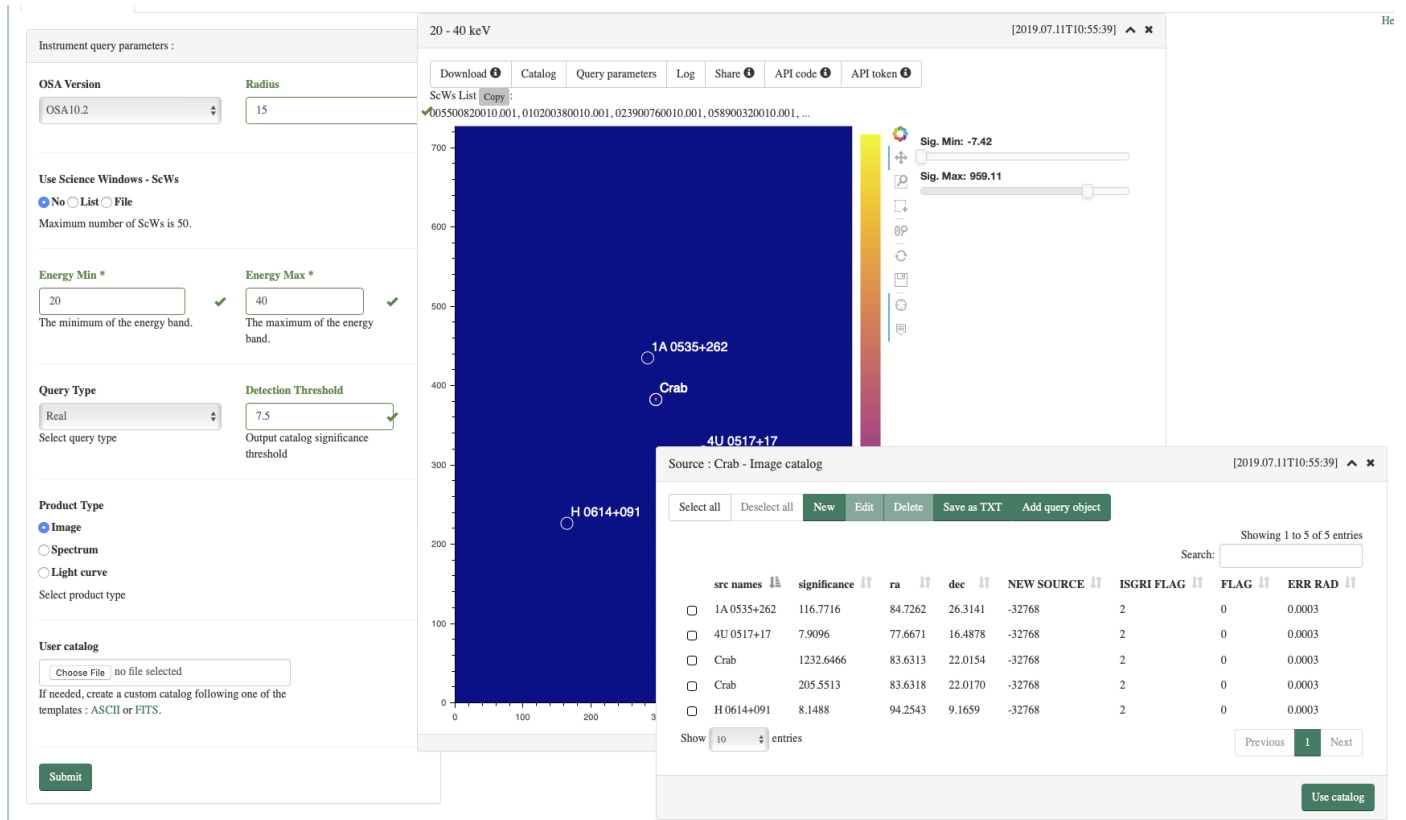


Fig. 4. Mosaic image of Crab region extracted from a sample of 50 randomly selected ScWs, together with the display of the catalog of detected sources. The result could be re-generated using the URL <https://doi.org/10.5281/zenodo.3634648>.

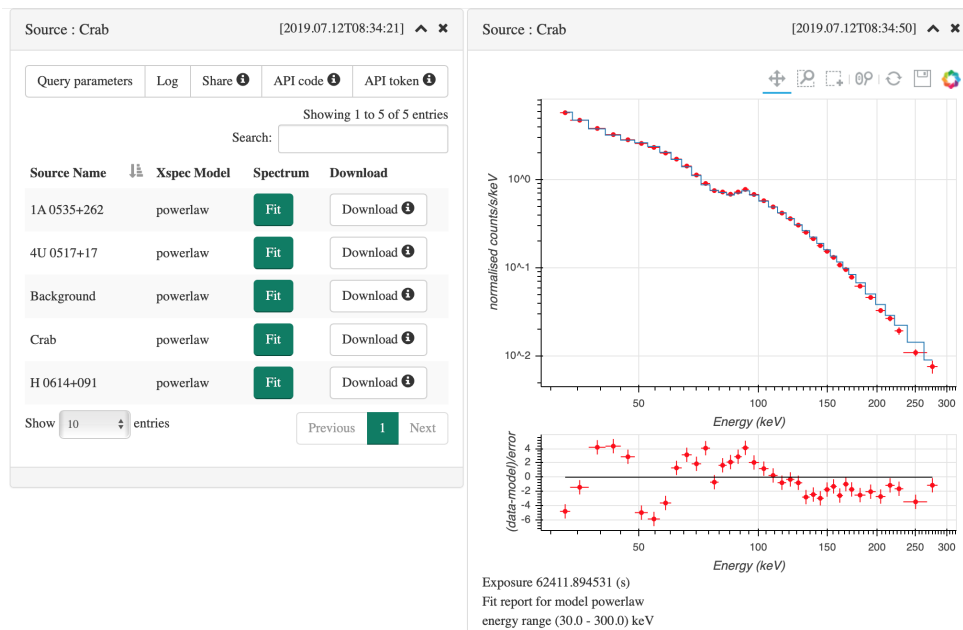


Fig. 5. Display of the Crab long-term (15 year time span) spectrum extracted from a sample of 50 randomly selected ScWs. The analysis could be re-generated via URL <https://doi.org/10.5281/zenodo.3634657>.

the search of sources in the mosaic and in individual ScWs. This might be important, because some flaring sources are detectable in individual ScWs during short time periods, but are not detectable in mosaic images with longer exposure times. The user is asked to carefully inspect the output catalog from the imaging step and adjust the source selection for the following spectral and timing analyses.

Imaging, spectral extraction and timing routines of OSA use catalogues of sources to match the shadow patterns corresponding to these sources on the detector plane. The catalog used for imaging, spectral or timing analysis could be explicitly specified in the “User catalog” parameter window in the parameter panel. If no user catalog is specified, the default general INTEGRAL catalog is used. This is advisable for the imaging products, but

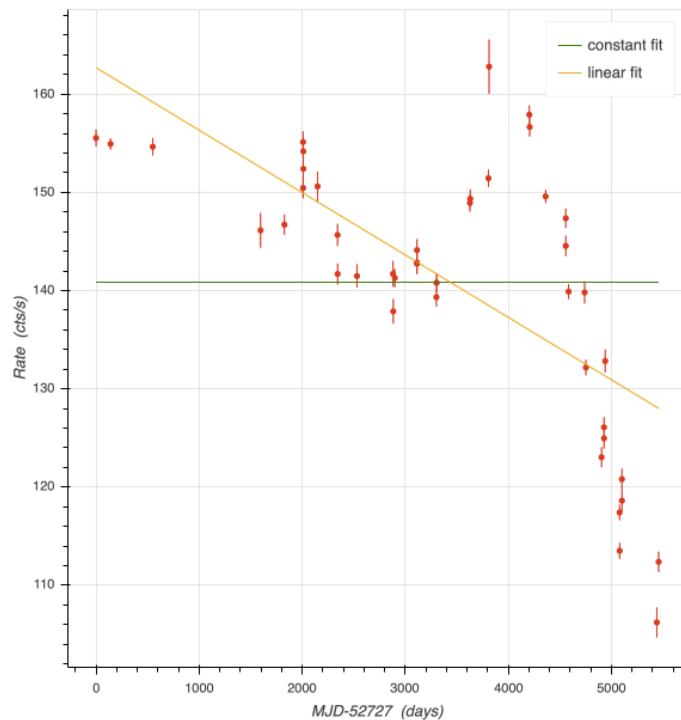
sub-optimal for the extraction of spectra and light curves, which relies on fitting a sky model on the shadowgram. If this sky model is redundant, the fitting becomes more problematic, resulting in unreliable flux determinations. The user can edit the catalog entries in the display of the catalog output of the imaging step. This display also has a “Use catalog” button, which would push the edited catalog to the “User catalog” to be used at the subsequent stages of analysis. The catalog can also be defined explicitly in the form of a python “dictionary” in the URL parameter field. The correctly formatted catalogue embedded in the URL can be obtained by clicking the “Share” button next to the displayed data product.

Fig. 5 shows the time-averaged spectrum computed using OSA version 10.2 for our example with a total exposure of 62 ks in 50 randomly selected ScWs. The display of results of spectral analysis for all sources listed in the catalog (user custom catalog or the output catalog from the imaging step analysis) provides a possibility to choose a spectral model for fitting the spectrum¹¹. Fig. 5 shows a fit of the Crab spectrum with a power law model. The display of the spectrum together with the fitted model also provides the details of the fit, such as the model parameter values with their uncertainties (the slope of the Crab spectrum found by the fit is $\Gamma = 2.091 \pm 0.003$) and the flux in 30-300 keV energy range ($2.186^{+0.004}_{-0.003} \times 10^{-8}$ erg/(cm²s).

The spectral properties of the Crab inferred with the ODA random selection of 50 ScWs are consistent with the “canonical” Crab spectrum in hard X-ray band (Mineo et al. 2006). Fig. 5 shows the spectral fit starting from 30 keV energy. The 20-30 keV band is the most affected by the long-term evolution of the ISGRI response, as the ISGRI energy threshold is gradually increasing with time and low-energy events are lost. For consistency, only data above 30 keV are thus automatically fitted, but data at lower energy are available, upon download of the FITS-format spectral file.

Fig. 6 shows the 30–100 keV light-curve of the source during a 17-years time span, extracted from the same set of 50 random ScWs and binned into ScW-long time bins. The figure shows the fit of the light-curve with constant and linearly changing flux models. There is a noticeable decrease of the source count rate toward later times, which becomes especially pronounced after MJD 56800 (mid-2014). Superimposed onto this instrumental trend, there is the true variability of the Crab nebula studied by Wilson-Hodge et al. (2011). Such rapid decrease of the count rate is due to the decrease of the instrument response at low energy and is not corrected in version 10.2 of OSA, because calibration algorithms were not able to correct this rapid evolution and calibration files were frozen at this moment. The correct instrument response after MJD 56800 is provided by version 11.0 of OSA with the relative calibration files¹². See Section 4 for details on the instrumental effects contributing to these results.

Fig. 7 shows a comparison of the long-term variability of the Crab flux in the 30–100 and 100–300 keV ranges for 17 years of INTEGRAL operations together with the ones measured by SWIFT/BAT and Fermi/GBM telescopes (Wilson-Hodge et al. 2011). To produce this figure, we select random sets of 50 ScWs spanning one year time intervals and extract ScW-by-ScW lightcurves by specifying 10 ks time steps in the ODA parameters for lightcurve time binning (this is longer than the duration of one ScW). These lightcurves are



Exposure 94905.98405 (s)

Fig. 6. Crab long-term (15 year time span) lightcurve extracted from a sample of 50 randomly selected ScWs in 30-100 keV band, using OSA10.2. The lightcurve is generated via URL <https://doi.org/10.5281/zenodo.3634664>.

subsequently averaged into the time bins used by Wilson-Hodge et al. (2011) for comparison. For this workflow, we exploited the API access to ODA platform, as coded in the [Crab_lc_longterm.ipynb](https://github.com/cdcihub/oda_api_benchmark) Jupyter notebook, which is part of the https://github.com/cdcihub/oda_api_benchmark GitHub repository. In Sect. 3.4, we detail how to run online Jupyter notebooks as the one used to produce Fig. 7.

From Fig. 7 one can see that the lightcurve extracted using OSA10.2 and OSA11.0 in their time intervals of validity are compatible with the lightcurves of SWIFT/BAT and Fermi/GBM, after they have been normalized to their average level. Intrinsic variability of the Crab nebula (at $\sim 5\%$ level) can be appreciated in the general trend of all instruments, as done by Wilson-Hodge et al. (2011). There is, however, some residual differences between the INTEGRAL and SWIFT/BAT or Fermi/GBM lightcurves, which can be used to estimate the systematic cross-calibration uncertainty. This amounts up to 10% in the 100-300 keV energy range.

Count rate light curve have variations that are also due to the evolution of the instrument gain; these are accounted for using response files to recover the intrinsic source flux in the spectral extraction stage. Table 1 shows the year-by-year change of the Crab spectrum measurements in 30-300 keV range, inferred from the Crab spectrum extraction from randomly selected sets of 50 ScWs in the time ranges shown in the first and second columns of the table. The flux is found to be stable to within $\pm 5\%$.

3.2. Extremely bright source: V404 Cygni

V404 Cygni is a microquasar that underwent a spectacular outburst in 2015 during which the source flux has reached 50 Crab

¹¹ Based on Xspec package fitting (<https://heasarc.gsfc.nasa.gov/xanadu/xspec/>).

¹² It is foreseen that the OSA11 software release will cover the full mission at the end of 2020.

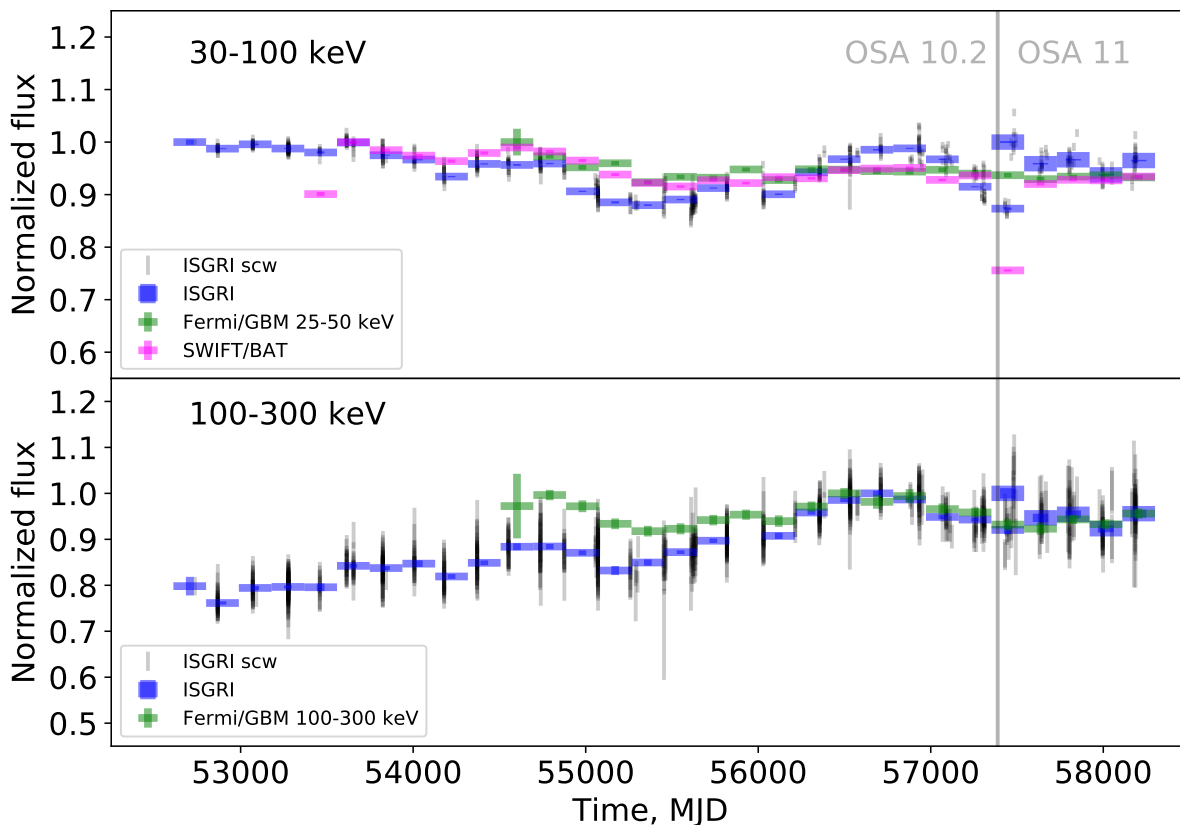


Fig. 7. Evolution of the Crab count rate over 17 years of INTEGRAL operations in 30-100 keV (top panel), 100-300 keV (bottom panel) energy ranges, compared to those observed by SWIFT/BAT (magenta) and Fermi/GBM (green data points) (Wilson-Hodge et al. 2011). Grey data points show the lightcurve binned in ScW by ScW time bins by the ODA. Blue blue data points show the rebinned individual ScW measurements. The reader can launch the Jupyter notebook [Crab_lc_longterm.ipynb](https://github.com/INTEGRAL/ODA/blob/master/notebooks/Crab_lc_longterm.ipynb) used to generate these long-term light curves via API access to ODA.

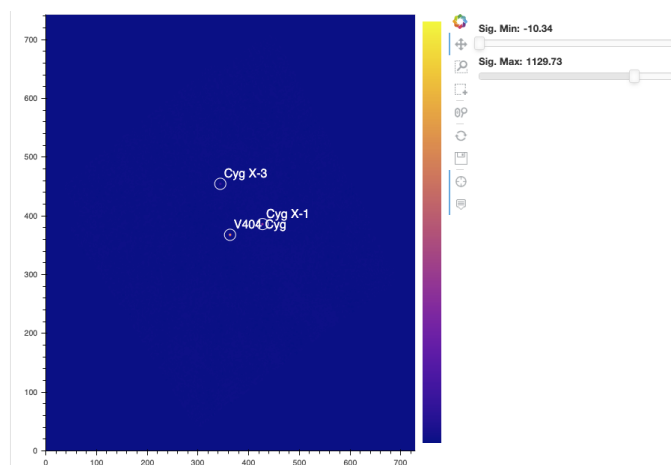


Fig. 8. Significance map of V404 Cygni region in 20-40 keV band. The image can be re-generated via URL <https://doi.org/10.5281/zenodo.3634669>.

(Sánchez-Fernández et al. 2017; Rodríguez et al. 2015). Such high flux might pose challenges for data analysis because of saturation or pileup effects that need to be properly taken into account.

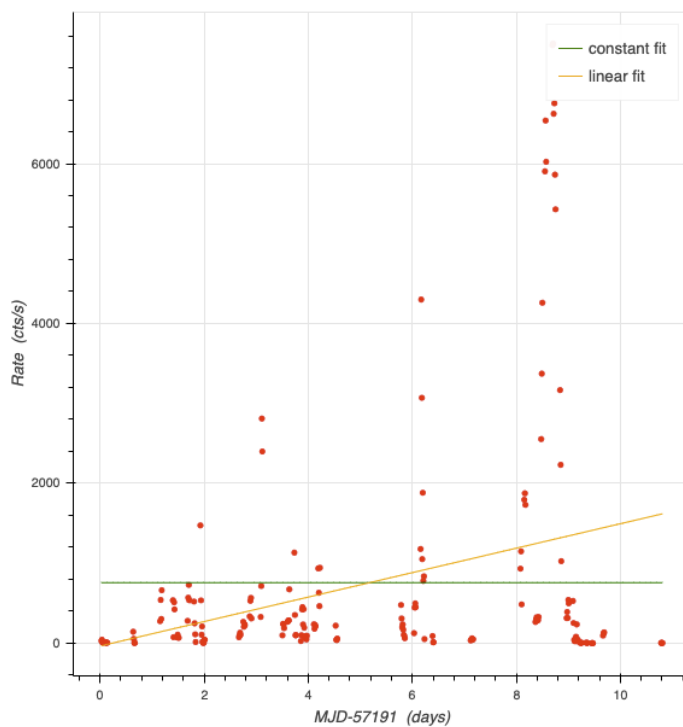
To validate the performance of ODA for the bright source case, we have reproduced the results of the analysis of V404 Cyg reported by Rodríguez et al. (2015).

At the first stage we assess the overall evolution of the source throughout the activity period that lasted from 2015-06-18T00:00:00.0 UTC to 2015-06-28T23:59:59.0 UTC. Entering this time interval into the ODA interface via the [the URL](#), we let the system select randomly 50 ScWs for the analysis with pointing directions within 10 degrees from the source direction and produce a mosaic image shown in Fig. 8. The source is the brightest one in the image detected with significance exceeding 1000σ . The next brightest source in the field is Cyg X-1. A very strong source produces “ghost” images due to the specific of the coded mask imaging technique. This could be readily seen in the example of V404 Cyg by extracting all the sources in the image detectable at significance threshold above 5σ : this would result in very large amount of “ghosts” that would appear in the resulting catalog as “NEW” sources.

Fig. 9 shows the lightcurve of V 404 Cyg extracted from the same 50 random ScW data set. Given the problem of detection of “ghost” sources around a very bright source, it is important to correctly define an input source catalog for the light curve production. Otherwise, the catalog that would be produced based on the imaging step of the analysis would include all the

Table 1. Evolution of the measurements of Crab flux and spectral slope over 15 years of observations.

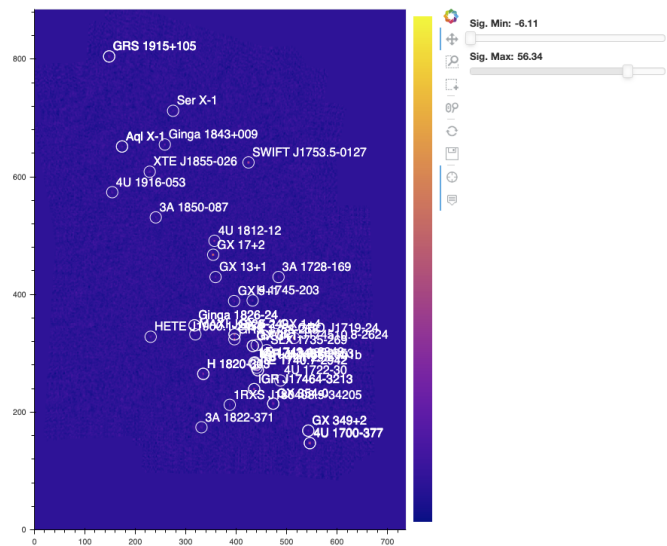
Start	Stop	Γ	F_{30-300} $\times 10^8 \text{ erg}/(\text{cm}^2\text{s})$	URL to
2003-03-15	2004-03-15	2.264 ± 0.002	2.066 ± 0.004	https://doi.org/10.5281/zenodo.3634693
2004-03-15	2005-03-15	2.089 ± 0.003	2.262 ± 0.005	https://doi.org/10.5281/zenodo.3634695
2005-03-15	2006-03-15	2.233 ± 0.003	2.084 ± 0.005	https://doi.org/10.5281/zenodo.3634709
2006-03-15	2007-03-15	2.093 ± 0.003	2.280 ± 0.003	https://doi.org/10.5281/zenodo.3634715
2007-03-15	2008-03-15	2.099 ± 0.003	2.286 ± 0.004	https://doi.org/10.5281/zenodo.3634725
2008-03-15	2009-03-15	2.089 ± 0.003	2.285 ± 0.005	https://doi.org/10.5281/zenodo.3634729
2009-03-15	2010-03-15	2.087 ± 0.003	2.277 ± 0.005	https://doi.org/10.5281/zenodo.3634735
2010-03-15	2011-03-15	2.096 ± 0.002	2.218 ± 0.004	https://doi.org/10.5281/zenodo.3634746
2011-03-15	2012-03-15	2.091 ± 0.003	2.259 ± 0.005	https://doi.org/10.5281/zenodo.3634742
2012-03-15	2013-03-15	2.089 ± 0.002	2.285 ± 0.004	https://doi.org/10.5281/zenodo.3634751
2013-03-15	2014-03-15	2.093 ± 0.002	2.259 ± 0.003	https://doi.org/10.5281/zenodo.3634754
2014-03-15	2015-03-15	2.093 ± 0.002	2.266 ± 0.003	https://doi.org/10.5281/zenodo.3634758
2015-03-15	2016-03-15	2.095 ± 0.002	2.276 ± 0.003	https://doi.org/10.5281/zenodo.3634760
2016-03-15	2017-03-15	2.026 ± 0.003	2.166 ± 0.004	https://doi.org/10.5281/zenodo.3634771
2017-03-15	2018-03-15	2.118 ± 0.003	2.068 ± 0.004	https://doi.org/10.5281/zenodo.3634773
2018-03-15	2019-03-15	2.123 ± 0.003	2.160 ± 0.005	https://doi.org/10.5281/zenodo.3634775


Fig. 9. Lightcurve of V404 Cygni during 2015 flaring period: [URL](#).

“ghost” sources in the procedure of fitting the detector image, which would lead to either wrong flux calculations or larger error estimates compared to the flux measurements including only real sources.

From Fig. 9, one can notice that the source underwent several short time flares. The time intervals of these flares are listed in Table 2. The overall evolution of the source flux inferred from ODA is consistent with that reported by Sánchez-Fernández et al. (2017); Rodríguez et al. (2015).

Rodríguez et al. (2015) have also reported variations of the source spectrum throughout the activity period. We have verified the spectral variability results with ODA by extracting the spectra for the time periods of the flares and for the “low flux” period during which the source count rate was below 10^3 cts/s (the same


Fig. 10. Significance map of the sky region around GX 17+2, [URL](#).

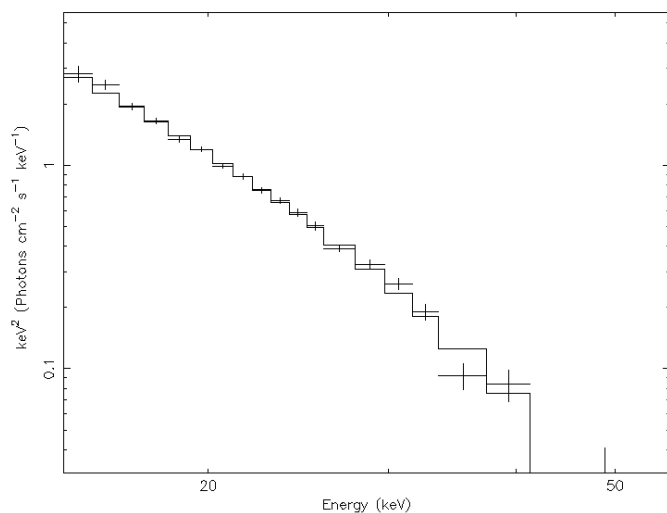
criterion for division on “low” and “high” as in Rodríguez et al. (2015)). Following Rodríguez et al. (2015) we have fitted the spectra with a cutoff powerlaw model. The results of the spectral fits are given in Table 2. The low and high flux state parameters are consistent with those reported by Rodríguez et al. (2015).

3.3. Crowded field: GX 17+2

To verify the performance of ODA in the crowded field, we consider an example of GX 17+2, a persistent bright low-mass X-ray binary with a neutron star. It is located in the inner Galaxy region in a “crowded” field with many bright sources. In such situation, OSA has to take into account simultaneously all the bright sources while modeling superposition of the shadows of different sources on the detector. If this is not done properly, the signal of the source of interest could be contaminated by the overlapping shadows of unaccounted sources. However, this is a minor concern for bright sources as contamination can reach at most a few percents of the contaminant’s flux in the worst cases.

Table 2. Time limits and spectral parameters extracted from the re-analysis of V404 2015 flare reported by [Sánchez-Fernández et al. \(2017\)](#).

State	Start	Stop	Exposure	Γ	E_{cut} keV	$F_{30-300} \times 10^9$ erg/(cm ² s)	URL
low	2015-06-18 00:00:00.0	2015-06-18 11:59:59.0	25 ks	1.02 ± 0.09	110 ± 15	4.22 ± 0.08	https://doi.org/10.5281/zenodo.3634785
high 1	2015-06-21 01:30:00.0	2015-06-21 04:29:59.0	3.8 ks	1.32 ± 0.02	60.7 ± 1.1	63.5 ± 0.2	https://doi.org/10.5281/zenodo.3634789
high 2	2015-06-24 02:30:00.0	2015-06-24 05:59:59.0	5.6 ks	2.578 ± 0.016	122 ± 4	55.26 ± 0.11	https://doi.org/10.5281/zenodo.3634796
high 3	2015-06-26 07:26:00.0	2015-06-26 21:29:59.0	14.4 ks	1.591 ± 0.007	93.1 ± 0.9	90.33 ± 0.10	This URL


Fig. 11. Time-averaged spectrum of GX 17+2 extracted from 50 randomly selected ScWs. The spectrum could be regenerated via [URL](#).

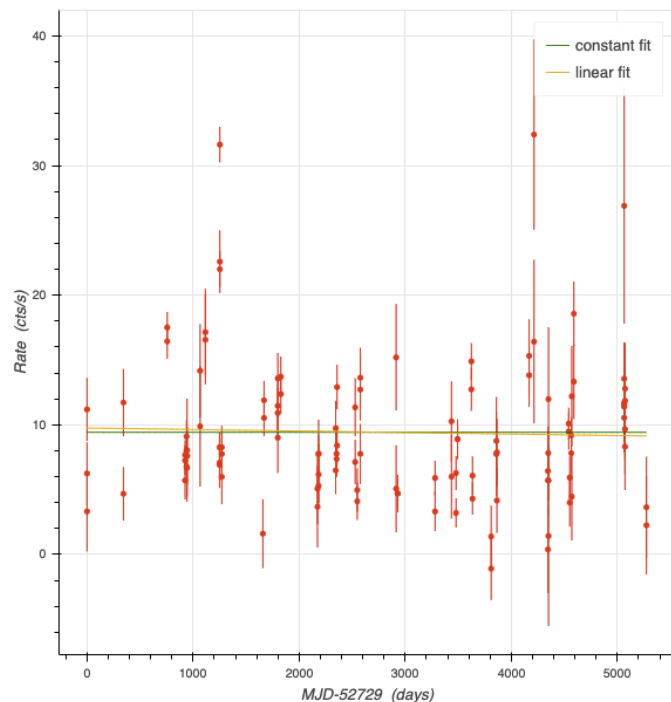
At the first stage of analysis, we selected a time interval spanning 15 years of INTEGRAL operations and let ODA select a random set of ScWs in which the source was less than 10° away from the center of the FoV. The resulting mosaic image of the field around the source is shown in Fig. 10. One can see that the imaging analysis has properly identified a large number of sources in the GX 17+2 region.

We have used the same set of ScWs to extract the spectrum of the source shown in Fig. 11. To reduce the computation time, we have used the catalog including only sources detected in the mosaic with significance larger than 30σ . The spectrum is consistent with a cut-off powerlaw. Fitting the spectrum in the energy range above 15 keV (this requires download of the spectrum, because the web interface uses 30 keV as default low-energy limit) one finds a very soft spectrum with spectral slope $\Gamma = 3.3 \pm 0.4$, cut-off energy $E_{cut} = 10 \pm 2$ keV and flux $(2.5 \pm 1.5) \times 10^{-10}$ erg/(cm²s) in 20–60 keV range.

The long-term evolution of the source flux is shown in Fig. 12. One can see that the source flux varies within a factor of two around the average level. It should be noted that the fractional variability level is much higher than that of Crab, so that the flux variations are much larger than the systematic uncertainty that can be derived from the Crab variability analysis.

3.4. 3C 279

The active galactic nucleus (AGN) 3C 279 is a weak source with hard spectrum in the INTEGRAL energy band. Its flux is at the level of the sensitivity limit of ISGRI and its detectability depends on the source state. One of the flaring episodes occurred in 2015 and INTEGRAL observations of 3C 279 dur-


Fig. 12. Light curve of GX 17+2 extracted from 50 random ScW set spanning 15 years: [URL](#).

ing this episode were obtained as a Target-of-Opportunity campaign. The results of data analysis for this TOO are described by [Bottacini et al. \(2016\)](#).

Following the same approach as for other sources, we first performed an exploration of the source behavior throughout the 15 year time span of the data. However, this source would likely be only marginally detected in any 50 ScW exposure, and no assessment of the variability pattern is possible in this way.

Instead, the full dataset has to be explored to find the periods during which the sources is detected. We use the API access to ODA to work with the datasets longer than 50 ScWs in the following way. As for the Crab lightcurve case in Sect. 3.1, the Jupyter notebooks for the 3C 279 analysis can be launched from the [cdcihub/oda_api_benchmark](#) GitHub repository, which is integrated with the Binder interactive notebook service¹³. [Launching the binder](#) using the “launch binder” button in the [cdcihub/oda_api_benchmark](#) repository and choosing the notebooks for 3C 279 lightcurve and spectra found in [examples](#) makes it possible to generate the results described below online.

At the first stage of analysis, we determine the bright sources in the source field. We generate a mosaic image of the field and use the output catalog of the mosaic analysis, adding explicitly 3C 279 to the catalog, as an input step for the timing and spectral

¹³ <https://mybinder.org>

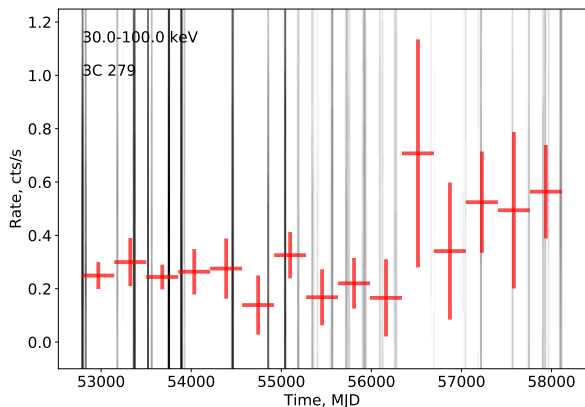


Fig. 13. Lightcurve of 3C 279 on 15 yr time span. Grey vertical lines show exposure periods of the source. The notebook [3C279_lc.ipynb](#) for the calculation of the lightcurve could be launched using this [URL](#).

analysis. Using the resulting source catalog, we process all sets of 50 ScWs in sequence to obtain a long-term lightcurve of the source shown in Fig. 13. From this figure one could see that the source is systematically detected throughout the entire 15 year time span. It shows moderate (if any) variability from year to year.

The 2015 flare of the source reported by [Bottacini et al. \(2016\)](#) is identifiable as the highest flux point in the lightcurve in Fig. 13. More detailed view of the lightcurve for the flaring episode discussed by [Bottacini et al. \(2016\)](#) is shown in Fig. 14. The average count rate is at the level of 1 ct/s, which agrees with the published value. This lightcurve can be re-generated using the same lightcurve extraction notebook as for the long-term lightcurve of the source, changing the time interval to focus on the flaring period, July 2015, and adjusting the energy range. This shows how the notebook available for on-the-fly re-deployment via the [cdcihub/oda_api_benchmark](#) web page can be re-used for refinement or re-use of the analysis for different energy ranges or different sources.

Fig. 15 shows a comparison of the time-averaged spectrum of the source with the flaring state spectrum. The spectral fit of the flaring state spectrum shown in Fig. 15 has a very hard slope $\Gamma = 0.7 \pm 0.3$, which is consistent with the results of [Bottacini et al. \(2016\)](#).

3.5. NGC 2110

NGC 2110 is an example of moderately bright Seyfert galaxy, i.e. a representative of typical hard X-ray bright and persistent AGN class ([Lubiński et al. 2016](#)). In this respect, it is different from the blazar-like 3C 279.

Fig. 16 shows the significance image of the source region extracted from a set of 50 random ScWs spread over 15 years of INTEGRAL operations. One can see that NGC 2110 is the brightest source in the field. Its detection significance reaches $\approx 17\sigma$ in the exposure $T \approx 90$ ks. The dimmer source H 0614+091 is detected at significance level 10σ , and there is no other source in the field detected with significance exceeding 5σ .

Fig. 17 shows the long-term lightcurve of the source extracted from the sequence of 50 ScW datasets pointed within 10 degrees from the source, using the same notebook as for the 3C 279 analysis, part of the [the cdcihub/oda_api_benchmark](#) repos-

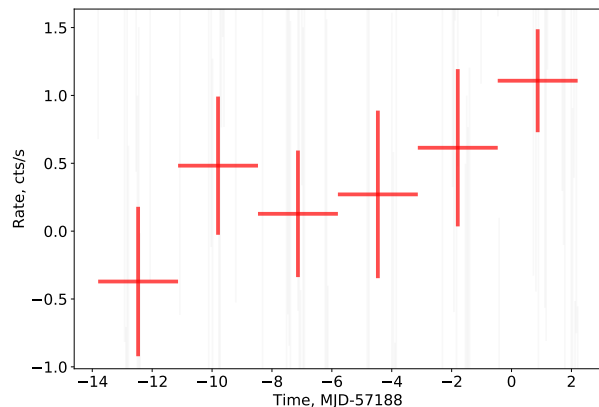


Fig. 14. Lightcurve of 3C 279 in 20-100 keV range for the flare period reported by [Bottacini et al. \(2016\)](#). The notebook [3C279_lc_flare.ipynb](#) for re-generation of the result can be executed online at this [URL](#), and is re-executable via Binder integration of cdcihub project.

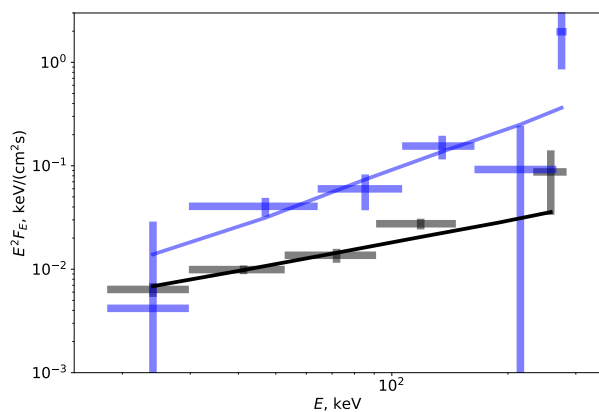


Fig. 15. Comparison of time-averaged spectrum of 3C 279 with the spectrum of the flaring state observed during the TOO period reported by [Bottacini et al. \(2016\)](#). The notebook [3C279_spectrum.ipynb](#) for the calculation of the spectra can be launched using this [URL](#).

itory. The statistical uncertainty of the flux measurement in individual ScWs is too large and it is not possible to follow the long-term evolution of the source spectrum with ScW-by-ScW binning. Taking this into account, we have rebinned the lightcurve into wider time bins. Several variability episodes are clearly identifiable with such binning in the long-term lightcurve.

We used the same approach as for 3C 279 for the extraction of the source spectrum with long exposure time. We extracted the spectrum of NGC 2110 stacking the spectra in sequences of 50 ScW long exposures and calculating the weighted average using the same notebook as for the extraction of the 3C 279 spectrum, available and executable at the [cdcihub/oda_api_benchmark](#) project page. The resulting source spectrum with a total exposure of 2.4 Ms is shown in Fig. 18. The figure shows two separate spectra for the periods of applicability of OSA 10.2 and OSA 11.0. The physical origin of the hard X-ray emission from Seyfert galaxies is thought to be due to the inverse Compton scattering of emission from an accretion disk in a hot corona characterized by certain temperature ([Lubiński et al. 2016](#)). Suppression of the emission above 100 keV expected in this model

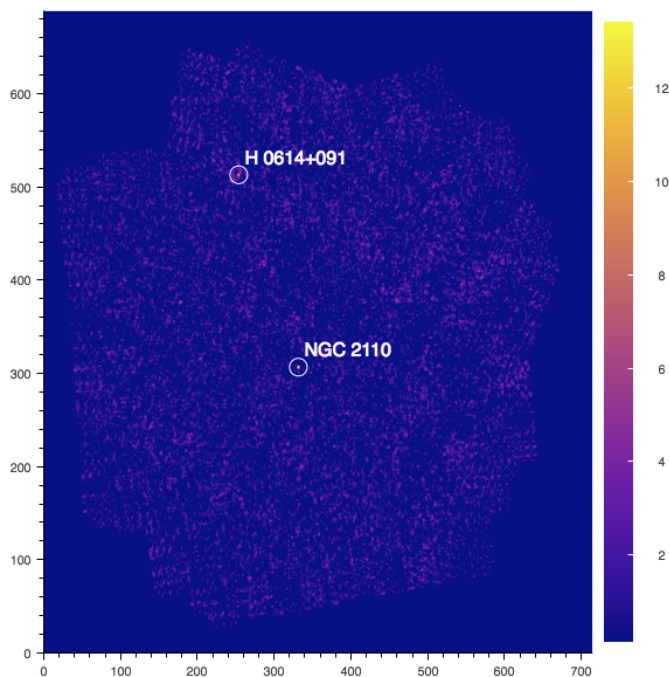


Fig. 16. 20-40 keV image of the NGC 2110 region extracted from a set of 50 randomly selected ScWs. The image could be regenerated via the URL <https://doi.org/10.5281/zenodo.3634584>.

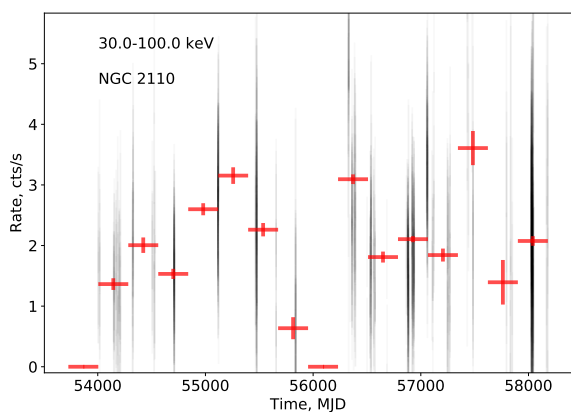


Fig. 17. Rebinned lightcurve of NGC 2110 extracted from the sequence of 50 ScW-long intervals using the notebook [lc_longterm.ipynb](#). The result could be re-generated via notebook deployment on Binder at this URL.

is seen in the longer (1.8 Ms) exposure spectrum for OSA 10.2 applicability period. However, the exposure of OSA 11.0 period (0.6 Ms) is not sufficiently long to constrain a high-energy cut-off in the spectrum.

4. Analysis limitations

In the current ODA implementation, the dispatcher defines which scientific analysis workflows can be executed through the frontend, and enables two versions of INTEGRAL analysis software: standard OSA10.2 and OSA11.0. OSA10.2 can only be used for the analysis of the data taken before 2016. OSA11.0 can only be used for the ISGRI data since 2016, while it can be used

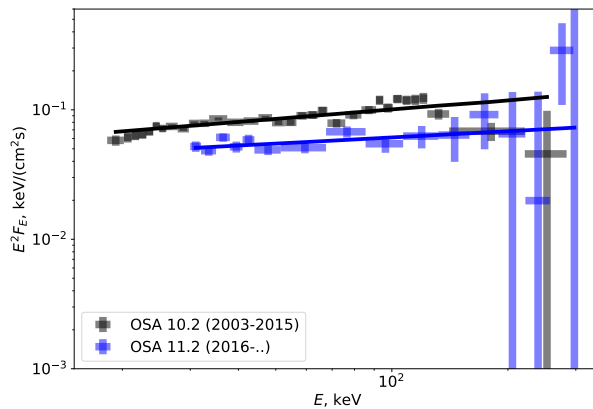


Fig. 18. Spectra of NGC 2110 extracted from the stacking of spectra obtained for 50 ScW sets in the time periods 2003-2015 (OSA 10.2) and from 2016 on (OSA11.0). The spectra can be re-generated online using the notebook [spectrum_longterm.ipynb](#). The result can be regenerated via notebook deployment on Binder via this URL.

for JEM-X during the full mission lifetime. This will change, as soon as updated ISGRI calibration files are made available.

The maximum number of ScW allowed in a single request is set to 50 (corresponding to up to 50 CPU-hours of computing), to reduce load on the system through too long jobs. This might change if the back-end is deployed in a different location or more computing resources are made available. Large requests will also be available for authenticated users. As of now, it is possible to overcome this limitation by looping over successive sets of 50 ScWs as it is demonstrated in the examples of analysis in this paper.

The INTEGRAL data analysis within ODA platform entirely relies on scientific data analysis with OSA, modifying only the mechanism with which individual components of OSA are invoked (principally to allow for preservation and re-use of intermediate analysis results, as explained above). It means that INTEGRAL analysis within ODA shares the limitations of OSA, and any future changes in OSA will be available in ODA.

Detailed scientific validation of the long-term evolution of the INTEGRAL instruments and the current status of the data analysis software with OSA goes beyond the scope of this paper, and will be a subject of a dedicated study following (Savchenko 2019).

For the purposes of this paper, we will only note that studies of source long-term evolution with INTEGRAL are known to be affected by substantial intrinsic evolution of the instrument, which can not be corrected without expanding a more recently developed instrument model used in OSA11 to the earlier mission, as show in in Savchenko et al. (2015). In particular, the meaning of the ISGRI rate and its relation to the reconstructed fluxes in different OSA versions is detailed in Savchenko (2020b). As advised by the OSA User Manual¹⁴, detailed long-term evolution should rely not on instrument rate but on the reconstructed flux, assuming additional 5% systematic uncertainty on the absolute flux reconstruction with ISGRI, as advised by the instrument team. On the other hand, this uncertainty is small comparing to intrinsic evolution of hard X-ray sources such as those studied in this paper.

¹⁴ <https://www.isdc.unige.ch/integral/analysis>

5. Conclusions

We have presented the new approach for the INTEGRAL data analysis which uses the cloud computing technology to enable deployment of data analysis workflows for imaging, spectral and timing analysis online through a web interface in a web browser: https://www.astro.unige.ch/cdci/astrooda_ or through a dedicated API that can be used in Python notebooks executable locally or remotely from the [cdcihub](#) project Github repository. Such an approach provides an important boost for reproducibility of results extracted from INTEGRAL data and possibilities of sharing and re-use of data analysis methods. Virtualisation of the data analysis system also provides a viable solution for the long-term preservation of the data and analysis results. This paper demonstrates how reusable astronomical data analysis workflows can be shared and embedded in publications.

Performance tests presented in this paper validate ODA for use in scientific publications making use of INTEGRAL data. ODA results are identical to those which are obtained with OSA with parameters choices following standard recommendations of the OSA hand books.

References

- Bottacini, E., Böttcher, M., Pian, E., & Collmar, W. 2016, *ApJ*, 832, 17
- Courvoisier, T. J.-L., Walter, R., Beckmann, V., et al. 2003, *A&A*, 411, L53
- Goldwurm, A., David, P., Foschini, L., et al. 2003, *A&A*, 411, L223
- Gupta, A. 2009, *Data Provenance*, ed. L. LIU & M. T. ÖZSU (Boston, MA: Springer US), 608
- Hester, J. J. 2008, *ARA&A*, 46, 127
- Ikeda, R. & Widom, J. 2009
- Labanti, C., Di Cocco, G., Ferro, G., et al. 2003, *A&A*, 411, L149
- Lebrun, F., Leray, J. P., Lavocat, P., et al. 2003, *A&A*, 411, L141
- Lubiński, P., Beckmann, V., Gibaud, L., et al. 2016, *MNRAS*, 458, 2454
- Lund, N., Budtz-Jørgensen, C., Westergaard, N. J., et al. 2003, *A&A*, 411, L231
- Mineo, T., Ferrigno, C., Foschini, L., et al. 2006, *A&A*, 450, 617
- Rodríguez, J., Cadolle Bel, M., Alfonso-Garzón, J., et al. 2015, *A&A*, 581, L9
- Sánchez-Fernández, C., Kajava, J. J. E., Motta, S. E., & Kuulkers, E. 2017, *A&A*, 602, A40
- Savchenko, V. 2019, *Reusable Cross-Calibration Workflows*, <https://zenodo.org/record/3559528>, 10.5281/zenodo.3559528
- Savchenko, V. 2020a, *PoS, Asterics2019*, 072
- Savchenko, V. 2020b, *Inter-OSA Rate Normalization for INTEGRAL ISGRI*, Zenodo, <https://zenodo.org/record/3667772>, 10.5281/zenodo.3667772
- Savchenko, V., Lebrun, F., & Laurent, P. 2015, in *Proceedings of 10th INTEGRAL Workshop: A Synergistic View of the High-Energy Sky — PoS(Integral2014)* (Annapolis, MD, USA: Sissa Medialab), 083
- Savchenko, V., Neronov, A., & Courvoisier, T. J.-L. 2012, *A&A*, 541, A122
- Ubertini, P., Lebrun, F., Di Cocco, G., et al. 2003, *A&A*, 411, L131
- Vedrenne, G., Roques, J.-P., Schönfelder, V., et al. 2003, *A&A*, 411, L63
- Westergaard, N. J., Kretschmar, P., Oxborrow, C. A., et al. 2003, *A&A*, 411, L257
- Wilson-Hodge, C. A., Cherry, M. L., Case, G. L., et al. 2011, *ApJ*, 727, L40
- Winkler, C., Courvoisier, T. J.-L., Di Cocco, G., et al. 2003, *A&A*, 411, L1